Journal of Crystal Growth 360 (2012) 105–110

Contents lists available at SciVerse ScienceDirect

Journal of Crystal Growth

journal homepage: www.elsevier.com/locate/jcrysgro

Crystal growth of rutile by tilting-mirror-type floating zone method

Satoshi Watauchi [a,*], Md. Abdur Razzaque Sarker [a], Masanori Nagao [a], Isao Tanaka [a], Takashi Watanabe [b], Isamu Shindo [b]

[a] Center for Crystal Science and Technology, University of Yamanashi, 7-32 Miyamae, Kofu, Yamanashi 400-8511, Japan
[b] Crystal Systems Co., 9633-1 Kobuchisawa, Hokuto, Yamanashi 408-0044, Japan

ARTICLE INFO

Available online 16 December 2011

Keywords:
A1. Defects
A1. Etching
A1. Interface
A2. Floating zone technique
A2. Growth from melt
B1. Oxide

ABSTRACT

Mirror tilting effects on the interface shape during crystal growth and on the etch pit density of the grown crystals were studied using a tilting-mirror-type image furnace. With increase of tilting angle of mirrors, convexities of both melt-feed and melt-crystal interface and the etch pit density of the grown crystal were systematically reduced. The melt zone, which is formed during crystal growth, was also stabilized by mirror tilting. In the mirror tilted condition, a large rutile single crystal of 19 mm ϕ diameter was successfully grown.

1. Introduction

Many industrial single crystals like silicon are manufactured by melt growth techniques such as the Czochralski and Bridgman methods. Large single crystals can be grown by these methods. However, the segregation control of the dopant is very difficult in these methods. The floating zone method has an advantage for segregation control. The use of the floating zone method, however, is limited because the diameter of the crystals grown by this method is usually smaller than the other melt growth techniques such as the Czochralski and Bridgman methods. Highly resistive silicon single crystals are manufactured by the rf-heating floating zone (rf-FZ) method. Rutile single crystals are manufactured by the infrared heating floating zone (IR-FZ) method because Rutile single crystals cannot be grown by the Czochralski method [1]. Although rutile single crystals are also manufactured by the Verneuil method, the etch pit density (EPD) of the rutile crystal grown by the IR-FZ method is one order of magnitude lower than that by of the same crystal grown by the Verneuil method [2]. Therefore, rutile single crystals grown by the IR-FZ method are useful for the optical device application.

Historically, the furnace for the IR-FZ method has been improved from the single-ellipsoidal-mirror-type image furnace to the four-ellipsoidal-mirror-type image furnace via the double-ellipsoidal-mirror-type image furnace. In the four-ellipsoidal-mirror-type-image furnace, a unique growth method named the anisotropic heating floating zone (AHFZ) method has been proposed [3,4,5]. However, the use of this method is mainly limited to studies in condensed matter physics such as that of high-T_c cuprates [6] because of the small diameter of the crystal grown by this method. The instability of the molten zone limits the diameter. In the growth of single crystals of large diameter, unexpected contact between the feed rod and the grown crystal often occurs even if the surface of the molten zone is melted. The stability of the molten zone is usually lost by this contact. This means that the interface shapes of both the melt–feed and the melt–crystal interfaces are convex. It is reported that interface shape can be controlled by controlling the rotation rate during crystal growth [7] and by using a heat reservoir [8,9]. However, the diameter of the grown crystal is not markedly improved.

Recently, we have noticed that the layout of the mirror and heating lamps is in the same horizontal plane and that this horizontal mirror symmetrical layout is not always necessary to form the molten zone. We assumed that this layout of the horizontal mirror symmetry is responsible for the horizontal mirror symmetrical convex interface shape of both the feed–melt and crystal–melt sides. If the mirrors are tilted as shown in Fig. 1, the fraction of heating light, which illuminates downward the molten zone, is expected to increase. Interface shape is also expected to change with mirror tilting. Therefore, we designed the tilting-mirror-type image furnace shown in Fig. 1 and investigated the mirror tilting effects on interface shape [10]. We found not only systematic change in interface shape but also a significantly stabilized molten zone. The stabilized molten zone makes it possible to grow the large rutile single crystal of diameter [10,11]. The characterization of the rutile single crystal grown by the tilting-mirror-type floating zone method revealed that etch pit density (EPD) is also reduced by the mirror tilting [12]. In this paper, a review of these results will be shown.

* Corresponding author. Tel.: +81 55 220 8656; fax: +81 55 254 3035.
E-mail address: watauchi@yamanashi.ac.jp (S. Watauchi).

0022-0248/$ - see front matter © 2011 Elsevier B.V. All rights reserved.
doi:10.1016/j.jcrysgro.2011.12.044

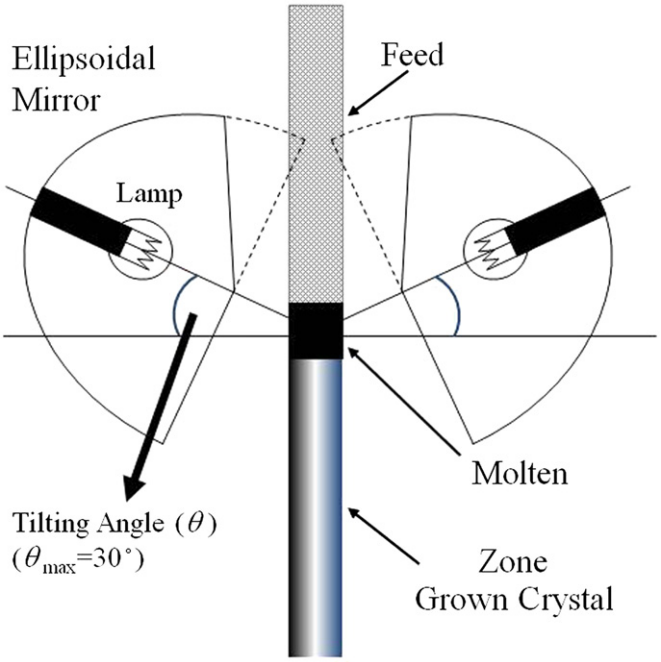

Fig. 1. Schematic illustration of tilting-mirror-type image furnace. The definition of tilting angle (θ) is given.

2. Experiment

A new tilting-mirror-type image furnace (Crystal Systems Corporation; model TLFZ-4000-H–VPO (Tilting FZ)) was developed for our study. The tilting angle θ, as shown in Fig. 1, can be changed up to 30° by a motor drive control. The upper parts of mirrors drawn in broken lines in Fig. 1 are eliminated to realize mirror tilting. Four halogen lamps of 1.5 kW were used for the growth of rutile.

2.1. Mirror tilting effects on interface shape during rutile crystal growth

High-purity rutile powder (> 99.99%) was placed in rubber tubes to form a rod shape and pressed at a pressure of up to 3.0×10^8 Pa using a cold isostatic pressing machine (Nikkiso Co., Ltd.: model CL3-22-60). The rods were sintered at 1600 °C for 12 h in an oxygen flow. When the sintered rods were used as feeds, the solidified molten zone was shattered during the cooling process after quenching the melt. Therefore, the sintered rods were zone-passed in a CO_2 flow at a growth rate of 25 mm/h using a standard four mirror-type-image furnace (Crystal Systems Corporation: model FZ-4000 H). The zone-passed feed rods were typically 6–11 mm in diameter and 70–100 mm in length.

Yttrium-doped rutile solvents were attached to the top edge of the zone-passed rods. As the segregation coefficient of yttrium in rutile was found to be much smaller than unity under the oxygen gas flow condition by one of our previous experiments, the doped yttrium in the molten zone hardly dissolves into the grown crystals and most of it remains in the quenched molten zone. Therefore, the shape of the solid–liquid interface will be evaluated by considering the yttrium distribution. The amount of yttrium-doped solvent was ~0.3 g. The concentrations of yttrium in the solvent were 0.1 at.% for $\theta=0°$ and 0.5 at.% for nonzero tilting angles because it was very difficult to maintain a stable molten zone of 0.5 at.% yttrium-doped solvent at $\theta=0°$.

The conditions for every growth and quenching experiment were a growth rate of 5 mm/h, a feeding rate of 5 mm/h, an upper shaft rotation rate of 3 rpm, a lower shaft rotation rate of 50 rpm, a growth direction of ⟨0 0 1⟩ using a rutile seed crystal, and an atmospheric-pressure oxygen flow. After reaching a growth length of ~25 mm, the molten zone was quenched by stopping the rotation of the shafts and turning off the heating lamps.

The quenched samples were cut at the center along the growth direction and polished finely to obtain mirror like surfaces. The yttrium distribution was characterized by X-ray microanalysis (XMA) (JEOL: model JXA-8200) to estimate solid–liquid interface shape.

To study the θ effects on interface shape, the rotation conditions and feed diameter were kept constant throughout the experiment to reduce the effects of both parameters on the θ effects on interface shape because the shape of the interface between the grown crystal and the molten zone is affected by rotation rate and feed diameter [7]. The pressed rods used as feed rods had a 10 (9.2–10.5) mmϕ at first. θ was changed in 5° increments up to 20°.

The diameter effects on interface shape were also investigated under both the nontilted condition of $\theta=0°$ and the tilted condition of $\theta=20°$. Crystal diameter was varied from 6 to 11 mm.

2.2. Trial growth of rutile single crystals of large diameter

For the growth of rutile single crystals of large diameter, a sintered rod of 10–12 mmϕ was used. At $\theta=20°$, rutile single crystals were grown at a rate of 5 mm/h in a CO_2 flow with a feeding rate of 5–15 mm/h because CO_2 flow is used for the commercial production of rutile crystals.

2.3. Mirror tilting effects on defects of grown rutile crystal

The rutile crystals were grown at three different θ's 0, 10, and 20° using a sintered rod of 10–11 mm diameter. The grown crystals were cut perpendicularly to the growth direction in the distance range of 22–25 mm from the seeding point. Then, the crystals were cut parallel to (1 0 0) and the surface was polished like a mirror. The polished samples were soaked in a mixture of $(NH_4)_2SO_4$ and H_2SO_4 solutions (1:1 weight ratio) for 3 h at 300 °C to etch their surfaces. The etch pits were observed by optical microscopy to obtain etch pit density (EPD). The EPDs of the larger rutile crystals, which are mentioned in Section 2, were also investigated in the same way.

3. Results and discussions

3.1. Mirror tilting effects on interface shape during rutile crystal growth

To obtain the solidified molten zone safely, the timing of turning the lamp off after stopping the rotation of both the upper and lower shafts was very important. A time of 2–3 s after stopping the rotation was good to turn off the lamps. When the time was too short, the solidified molten zone shattered during the cooling process. On the other hand, a melt drop occurred before turning off the lamps when the time was too long. This implies that the interface shapes obtained by the yttrium distribution mapping images might differ from the true interface shape during the crystal growth.

Fig. 2 shows SEM and yttrium distribution mapping images of the quenched samples for various tilting angles from $\theta=5°$ (a) to 20° (e). The signal of yttrium was detected as bright spots in yttrium mapping images. Most of yttrium was found to remain in the molten zone. The shapes of the solid–liquid interfaces could

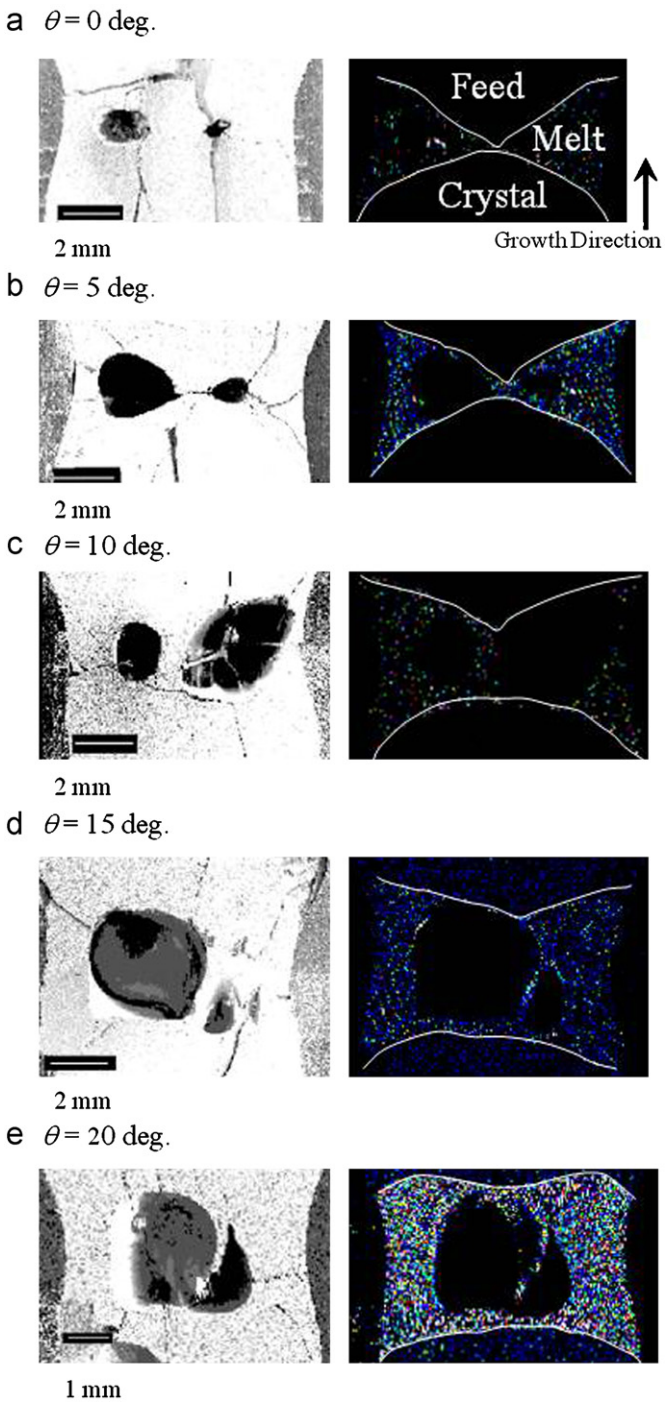

Fig. 2. SEM images (left) and yttrium distribution images (right) of quenched molten zones [$\theta=0^\circ$ (a), $\theta=5^\circ$ (b), $\theta=10^\circ$ (c), $\theta=15^\circ$ (d), and $\theta=20^\circ$ (e)]. Yttrium signals detected as bright spots in the molten zone were more than those in both the feed and the crystal. The solid–liquid interfaces were drawn as white lines for eye guide.

be observed clearly in yttrium distribution mapping images although they could not be observed in SEM images. The shapes of the solid–liquid interface on both the feed and grown-crystal sides were significantly affected by θ.

At the center of the quenched molten zone, one or two large bubbles 1–2 mm diameter are observed for all the samples. The origin of the bubbles is not yet clear. One possible origin is oxygen gas. Oxygen gas might have been formed by the reduction of some of the Ti^{4+} ions in the molten zone. Systematic trends in the number and location of the bubbles were observed. For larger θ's, (15° and 20°), a large bubble was observed at the center of the molten zone, and for smaller θ's, (0°, 5°, and 10°), two bubbles were observed. The reason for this is not yet clear. However, the changes in the number and location of bubbles imply that not only the shape of the interface on both the feed and grown-crystal sides but also the convection in the molten zone was greatly affected by the mirror tilting.

To carry out a quantitative investigation of the convexity of the solid–liquid interface between the molten zone and the grown crystal or the zone-passed feed, h/r was defined, where h is the height of the interface and r is the radius of the grown crystal or zone-passed feed, as shown in the schematic drawing of Fig. 3(c). The θ dependences of the convexities of the grown-crystal and feed sides obtained using the zone-passed feeds of $\sim$10 mmϕ are shown in Fig. 3(a) and (b), respectively. The diameter dependences of the convexities h/r of both the crystal and feed sides for $\theta=0^\circ$ and $\theta=20^\circ$ are also shown in Fig. 3(d) and (e), respectively.

At $\theta=0^\circ$, the observed convexities are smaller than those at a seed rotation rate of 20 rpm for the crystal of 10 mm in diameter, as reported by Higuchi and Kodaira [7]. In their case, rutile crystals were grown using a double-mirror-type image furnace under a CO_2 flow. The rotation rates of the feed and the seed were 30 rpm and 20–60 rpm, respectively. The high rotation rates of the seed, such as 40 rpm and 60 rpm, affect the convexity significantly for the crystal of 10 mm diameter. Either of these parameters might have affected the convexity in our experiments.

As we have already mentioned above, the rotation rates of the feed and seed were 3 rpm and 50 rpm in all our experiments. The convexity of the grown-crystal side decreased with increasing θ as shown in Fig. 3(a). This result indicates that the convexity can be systematically controlled by adjusting θ. Even at θ of 20°, the interface was still slightly convex. The growth at θ larger than 20° could not be examined because the zone-passed feed could not be melted using the lamp even at a full power of 6.0 kW (1.5 kW $\times$ 4). The most suitable lamp power for the crystal growth increased from 84% to 93% as θ increased from 0° to 20°, as shown in Fig. 4. On the other hand, the convexity of the feed side was also significantly dependent on θ, as shown in Fig. 3 (b). The feed-side convexity decreased more significantly than the grown-crystal side convexity with increasing θ. For $\theta=20^\circ$, the convexity was zero according to the definition of h/r, shown in Fig. 3(c). However, the interface was not completely flat; some areas of the interface were rather concave as shown in Fig. 2(e). In Fig. 5, the aspect ratio of the melt (L_P/D) and the normalized gap of the feed and crystal (L_C/D) are also shown. The definitions of L_P, L_C, and D are shown in Fig. 3(c). Both the aspect ratio of the melt and the normalized gap increased with θ.

In the conventional FZ, the interface shapes of both the feed and grown crystal sides are assumed to be convex, as shown in Fig. 3(c). This implies that not only the configuration of the heating lamps and the molten zone but also the shape of the molten zone has horizontal-mirror symmetry. The directions of the focusing rays are limited because the mirrors are parts of the ellipsoid. If the symmetric configuration of the heating lamps and the molten zone significantly affect the symmetric zone shape, as shown in Fig. 3(c), zone shape can be changed by tilting the mirrors because the melt is heated asymmetrically. First, the convexity of the grown-crystal side was expected to decrease and that of the feed side was expected to increase with increasing θ. The aspect ratio of zone shape L_P/D was also expected to increase with increasing θ. The normalized gap L_C/D was expected to be constant with increasing θ. Although the observed behaviors of the convexity of the grown-crystal side and the aspect ratio of the melt L_P/D were consistent with our simple expectations, as shown in Figs. 3(b) and 5, the observed behaviors of the convexity of the

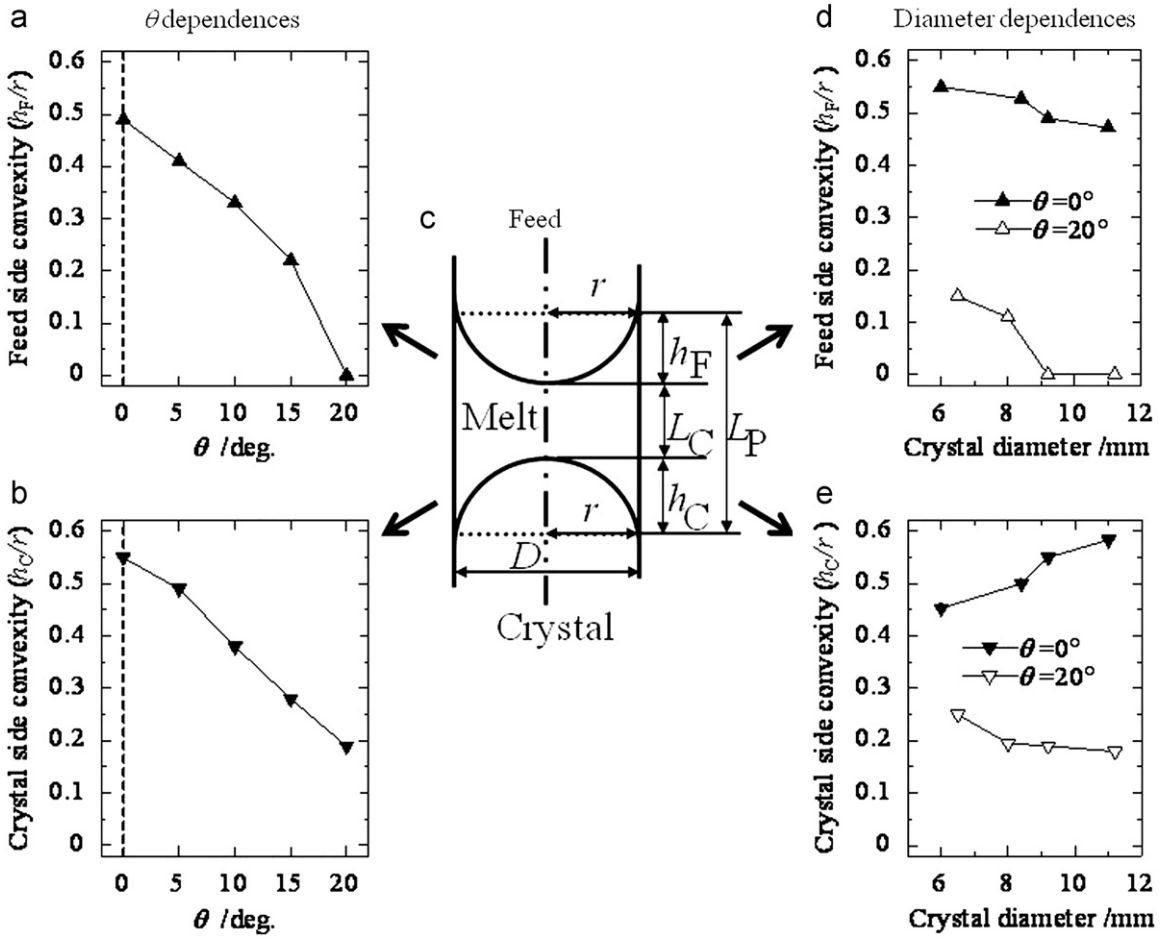

Fig. 3. Convexity (h/r) as function of tilting angle θ [feed side (a) and crystal side (b)]. Schematic illustration showing the definitions of h/r and L/D (c). Convexity (h/r) as function of crystal diameter [feed side (d) and crystal side (e)].

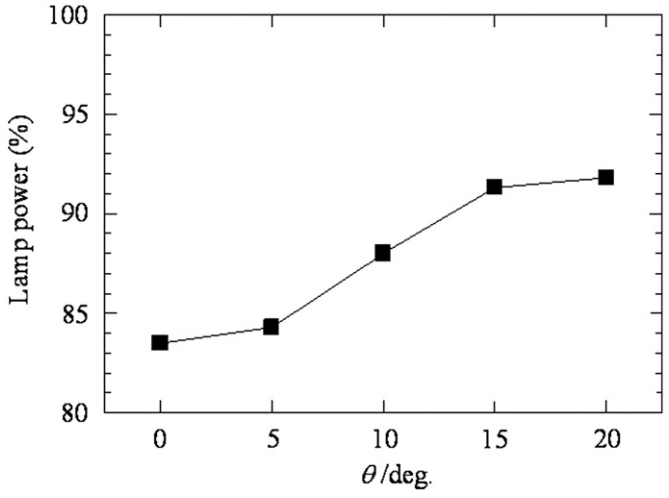

Fig. 4. Lamp power for growth as function of tilting angle θ.

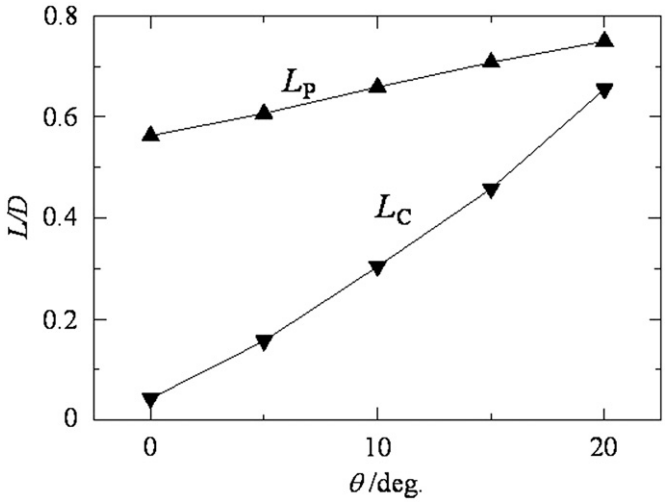

Fig. 5. Aspect ratio of melt (L_P/D) and normalized gap of feed and crystal (L_C/D) as functions of tilting angle θ.

feed side and the normalized gap L_C/D were quite different from our expectation, as shown in Figs. 3(a) and 5, respectively. The convexity of the feed side significantly decreased with increasing θ. This suggests that the convection in the molten zone is affected by θ because some areas of the feed-side interface were rather concave, as shown in Fig. 2(e). The increase in the normalized gap L_C/D with increasing θ suggests that the molten zone can be maintained using a lower lamp power. However, the lamp power, as shown in Fig. 4, was as low as possible to form a stable molten zone at each θ. The contact between the feed and the grown crystal occurred at a lower lamp power. These results suggest that the real increase in the normalized gap L_C/D with increasing θ is not as much as that shown in Fig. 5. As mentioned above, a time of 2–3 s after stopping the rotations of the feed and crystal was necessary before turning off the lamps to obtain a solidified

molten zone safely. The unexpected behaviors of both the convexity of the feed side and the normalized gap L_C/D might be caused by this timelag.

The stability of the molten zone appeared to increase even when θ was increased to 5° and the molten zone became more stable at a larger θ although it is very difficult to discuss it quantitatively. The stability of the molten zone is considered to correlate with the convexity of the grown-crystal side.

Fig. 3 (d) and (e) show the diameter dependences of the convexities of both the feed and crystal sides. At $\theta=0°$, the convexity of the feed side decreased from 0.55 to 0.47 with increasing crystal diameter from 6.0 to 11.0 mm, whereas that of the crystal side increased from 0.45 to 0.58. On the other hand, at $\theta=20°$, the convexity of the feed side decreased from 0.15 to 0.0 and that of the crystal side also decreased from 0.25 to 0.17 with an increase in diameter from 6.5 to 11.2 mm.

The behavior of the convexity of the crystal side at $\theta=0°$ enhances the possible collapse of the molten zone during the growth of a crystal of larger diameter. On the other hand, that at $\theta=20°$ means that the molten zone is rather stabilized during the growth of a crystal of larger diameter. Although the reason for the different behaviors of the convexities is not yet clear, the convections in the molten zone such as the forced convection and Marangoni convection must play an important role in such behaviors. The forced convection caused by the crystal rotation is dominant in the melt above the core region, and the convection flows in the centrifugal direction. The Marangoni convection is driven by the surface tension gradient due to the temperature gradient. It is dominant in the melt above the peripheral region and flows in the direction from the edge to the core [13]. In our experiments, however, no clear evidence for discussing convection in the molten zone is obtained.

3.2. Trial growth of rutile single crystals of large diameter

Fig. 6 shows photographs of the molten zone and the corresponding grown crystals of (a) 10, (b) 16, and (c) 19 mm diameters. Large crystals were successfully grown under the tilted condition of $\theta=20°$. In the growth of a 10 mmϕ crystal, the feeding speed was 5 mm/h, which was the same as the growth speed. However, in the growth of 16 mmϕ and 19 mmϕ crystals, a higher feeding speed of 15 mm/h was applied to increase crystal diameter. The diameters of the feeds for the growth of 16 mmϕ and 19 mmϕ crystals were 10 and 12 mm, respectively. The photographs taken during the growth indicate that the trapezoidal molten zone was maintained stably during the crystal growth.

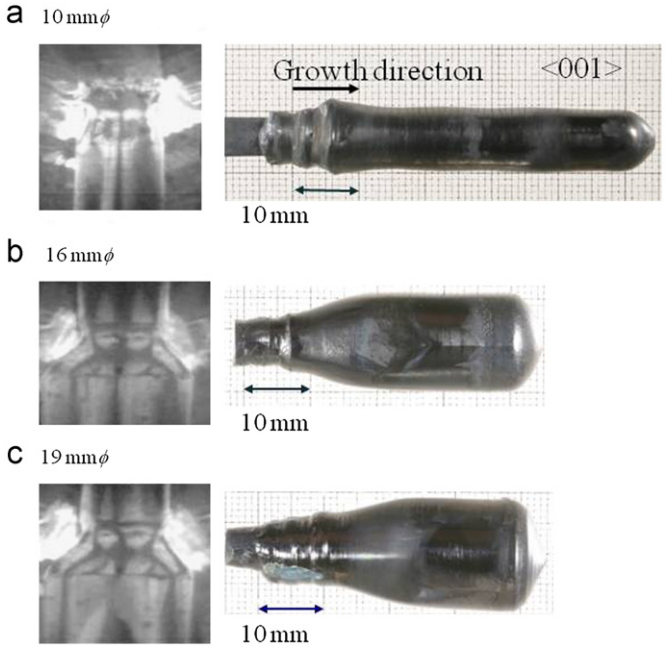

Fig. 6. Photographs of molten zone during crystal growth and photographs of grown crystals of (a) 10, (b) 16, and (c) 19 mm diameters.

3.3. Mirror tilting effects on defects of grown crystal

Fig. 7 shows plots of the EPD on the (1 0 0) surface as a function of the radius position, X, for the crystals of various diameters grown at various θ's. For all the crystals, the EPDs at the center were lower than those at the periphery. Sn-doped PbTe single crystals grown by the Bridgman method [14] showed a similar distribution of etch pits. In our case, the observed EPDs of the 10 mmϕ crystal grown at $\theta=0°$ ranged from 5×10^4 to 16×10^4 cm^{-2}, as shown in Fig. 7. These values are close to the reported EPDs of 7×10^4 cm^{-2} on the (1 1 0) plane for the rutile single crystals grown by the FZ method using a conventional image furnace with double ellipsoidal mirrors [2]. The EPDs systematically decreased at both the periphery and the center with increasing θ. The EPD at the center of the rutile crystals grown at $\theta=20°$ was minimum at 1.5×10^4 cm^{-2}, which was almost independent of the diameter of rutile crystal grown at $\theta=20°$. The EPD at the periphery also seems to be independent of crystal the diameter, although slightly lower for the 16 mmϕ grown crystal.

As EPD is associated with crystal quality because EPD arises from dislocation density [15], the above results show that the quality of the grown crystals was improved by the mirror tilting and that crystal diameter did not affect the quality of the grown crystal. As mentioned above, the convexity of the solid–liquid interface between the melt and the grown crystal decreased with increasing θ. A less convex interface was realized at $\theta=20°$ than at $\theta=0°$, which shows the same alignment of mirrors as that in the conventional experiments. An extremely convex interface is

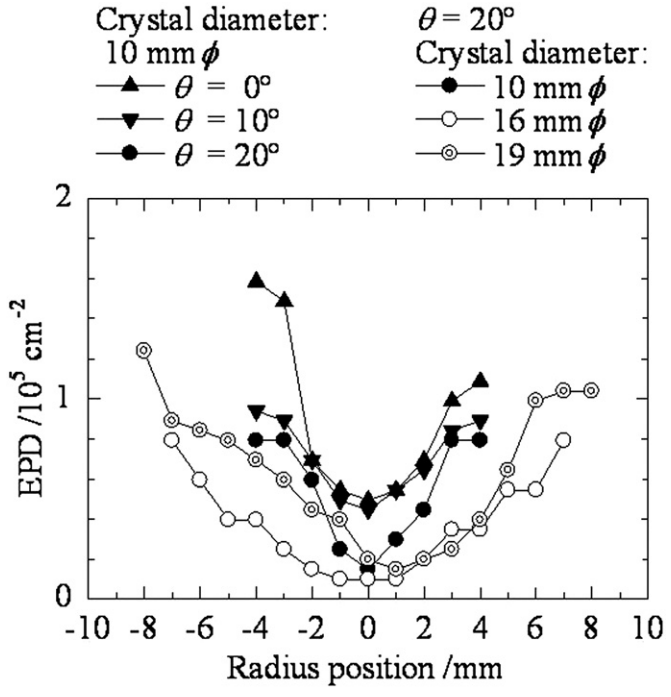

Fig. 7. Distributions of etch pit density as function of radius position (X) of crystals with different diameters grown at different θ's.

unfavorable for the growth of crystals with a low defect density because of the large number of defects caused by thermal stress [7]. Kitamura et al. found that line defects propagate to the edge of a crystal if the solid–liquid interface is more convex toward the melt [16]. Kinoshita and Sugii showed that the numbers of low-angle grain boundaries are markedly reduced when the solid–liquid interface during crystal growth is almost flat [14]. A slightly convex interface toward the melt is better for improving the quality of the grown crystals [17]. The slightly convex interface was achieved by tilting the mirror at $\theta=20^{\circ}$, as shown in Fig. 3 (b). The behavior of EPDs observed in our present experiment is consistent with these reported results.

Thus, we can conclude that the tilting angle of the mirrors used in crystal growth is an important factor for controlling defects in rutile crystals grown by the FZ method using an infrared heating image furnace and that high-quality crystals with a large diameter can be grown under a mirror tilted condition ($\theta=20^{\circ}$).

4. Conclusions

The shape of the molten zone during rutile crystal growth by the floating zone method using a tilting mirror type image furnace and the etch pit density distribution of the grown rutile crystal were studied. The convexity of the crystal-side interface decreased with increasing θ. The stability of the molten zone was also enhanced. The etch pit distribution revealed that the quality of the grown crystal was significantly improved during its growth under the mirror tilted condition. A large rutile single crystal of 19 mmϕ diameter was also successfully grown under the mirror tilted condition. These results indicate that the small crystal diameter, one of the largest disadvantages of the IR–FZ method, is improved by mirror tilting.

Acknowledgements

This work was partially supported by the Nippon Sheet Glass Foundation for Materials Science and Engineering, the Sasagawa Science Foundation Program (No. 21-332) of the Japan Science Society (JSS), and a Grant-in-Aid for Scientific Research (C) (No. 20550173) from the Japan Society for the Promotion of Science (JSPS).

References

[1] H. Machida, T. Fukuda, Journal of Crystal Growth 112 (1991) 835–837. CZ-TiO2 X.
[2] M. Higuchi, T. Hosokawa, S. Kimura, Journal of Crystal Growth 112 (1991) 354–358.
[3] S. Watauchi, M. Wakihara, I. Tanaka, Journal of Crystal Growth 229 (2001) 423–427.
[4] D.H. Kwon, S. Watauchi, M. Nagao, I. Tanaka, Journal of Crystal Growth 311 (2009) 4535–4537.
[5] D.H. Kwon, S. Watauchi, M. Nagao, I. Tanaka, Crystal Research and Technology 45 (2010) 692–696.
[6] I. Tanaka, H. Kojima, Nature 337 (1989) 21–22.
[7] M. Higuchi, K. Kodaira, Materials Research Bulletin 29 (1994) 545–550.
[8] K. Kitamura, S. Kimura, K. Watanabe, Journal of Crystal Growth 57 (1982) 475–481.
[9] S. Watauchi, I. Tanaka, K. Hayashi, M. Hirano, H. Hosono, Journal of Crystal Growth 237-239 (2002) 801–805.
[10] M.A.R. Sarker, S. Watauchi, M. Nagao, T. Watanabe, I. Shindo, I. Tanaka, Journal of Crystal Growth 312 (2010) 2008–2011.
[11] M.A.R. Sarker, S. Watauchi, M. Nagao, T. Watanabe, I. Shindo, I. Tanaka, Journal of Crystal Growth 317 (2011) 135–138.
[12] M.A.R. Sarker, S. Watauchi, M. Nagao, T. Watanabe, I. Shindo, I. Tanaka, Crystal Growth and Design 10 (2010) 3929–3930.
[13] K. Kitamura, N. Ii, I. Shindo, S. Kimura, Journal of Crystal Growth 46 (1979) 277–285.
[14] K. Kinoshita, K. Sugii, Journal of Crystal Growth 71 (1985) 283–288.
[15] W.M. Hirthe, J.O. Brittain, Journal of the American Ceramic Society 45 (2006) 546–554.
[16] K. Kitamura, S. Kimura, S. Hosoya, Journal of Crystal Growth 48 (1980) 469–472.
[17] C.H. Chiang, J.C. Chen, Journal of Crystal Growth 294 (2006) 323–329.